11

Application of Molecular Dynamics Simulations to Plasma Etch Damage in Advanced Metal-Oxide-Semiconductor Field-Effect Transistors

Koji Eriguchi
Graduate School of Engineering, Kyoto University
Japan

1. Introduction

According to "the international technology roadmap for semiconductors (ITRS)" (SIA, 2009), the shrinkage of silicon-based metal–oxide–semiconductor field-effect transistor (MOSFET) – an elemental device (unit) in ultra-large-scale integrated (ULSI) circuits – has been accelerating due to expanding demands for the higher performance and the lower power operation. The characteristic dimensions of current MOSFETs in mass productions are around 30 – 50 nm. Figure 1 shows the scaling trend of the key feature sizes in ULSI circuits predicted by Semiconductor Industry Association, USA. Various types of MOSFETs are designed for the specific purposes, i.e., low standby power (LSP), low operation power (LOP), and high performance (HP) operations, and built in ULSI circuits such as dynamic random access memory (DRAM) and micro-processing unit (MPU). New structured MOSFETs such as fully-depleted (FD) and metal-gate (MG) devices have been recently proposed. Since physical gate length (*Lg*) and source / drain extension depth (Ext) are the key feature sizes determining MOSFET performance (Sze & Ng, 2007), the shrinkage of *Lg* and Ext is a primal focus in the development of MOSFETs. These sizes have become a few nanometers, comparable to the scale of atomistic simulation domain.

To meet the requirements such as fabricating fine patterns with anisotropic features, plasma etching is widely used in mass production of MOSFETs. At present, the control of the pattern transfer by plasma etching needs to be within the variation of a few nanometers (SIA, 2009). In such regimes, the feature size of the region where plasma - etch reactions are occurring becomes no more negligible with respect to the scale of MOSFET. Thus, precise control of the surface reaction between plasma and device is strongly required. In plasma etch process, radicals (atoms or molecules in an excited state) react with surface material with a help of the energy of incident ions accelerated in the "sheath" between plasma and device surface. This reaction mechanism is commonly referred to as "reactive ion etching (RIE)" (Lieberman & Lichtenberg, 2005). In some plasma etch processes, an energy of the ion becomes larger than 1 keV to obtain high etch rate. In such schemes, an unexpected reaction may occur. This unexpected ("unwanted") reaction mechanism is usually called as "plasma process-induced damage" (Eriguchi & Ono, 2008; Lieberman & Lichtenberg, 2005; Oehrlein, 1989), which is bringing out many key problems in the development of MOSFETs.

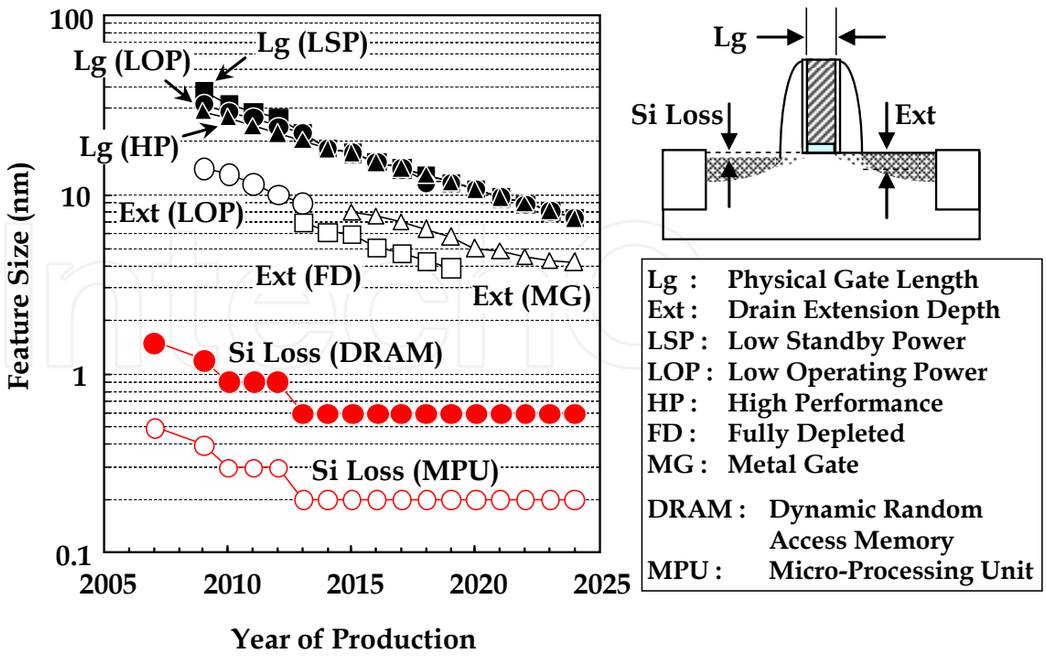

Fig. 1. Scaling trend of feature sizes in a metal–oxide–semiconductor field-effect transistor (MOSFET) in an ultra-large-scale integrated circuit.

Plasma process-induced damage (PID) is one of the serious issues causing degradation of MOSFET performance and reliability. Figure 2 illustrates an example of PID during a typical plasma etch process. Si wafer is placed on a wafer stage in a plasma chamber. Reactive plasma is generated by power supply. This figure corresponds to an inductively coupled plasma (ICP) system (Lieberman & Lichtenberg, 2005), where powers with frequencies of f_1 and f_2 are supplied to a plasma source (f_1) and a wafer stage (f_2), respectively. During plasma etching, MOSFET is exposed to a plasma and energetic ions impact on the surface. This energetic ion bombardment results in creation of defects (*ex.* displaced Si atom) in the Si surface region of MOSFET. This mechanism is one of examples of PID (Eriguchi & Ono, 2008). During more than the last two decades, PID has been studied extensively to understand the mechanisms and to solve practical problems with various approaches. In order to obtain the statistical data in mass production and to clarify the source of PID, a use of specifically designed devices called "test elementary group (TEG)" (SIA, 2009) has been a major approach. In addition to the use of TEG, physical and electrical analyses have been conducted by using a bare Si wafer to gain fundamental understanding of PID. To realize future high-performance MOSFETs, understanding and controlling (minimizing) PID is crucial because the critical dimension of reaction-layer thickness and device feature size will be in conflict with the plasma-damaged-layer thickness governed by plasma parameters. In other words, the damaged-layer thickness does not scale with device- shrinkage trends shown in Fig. 1.

Several simulation techniques have been proposed so far for plasma etch process. There are two major schemes: (1) Plasma-etch feature-profile simulations employing a small cell (Jin et al., 2002; Tsuda et al., 2011) and (2) Surface-reaction simulations based on a molecular dynamics (MD) (Graves & Humbird, 2002; Ohta & Hamaguchi, 2001a, 2001b; Sankaran & Kushner, 2004).

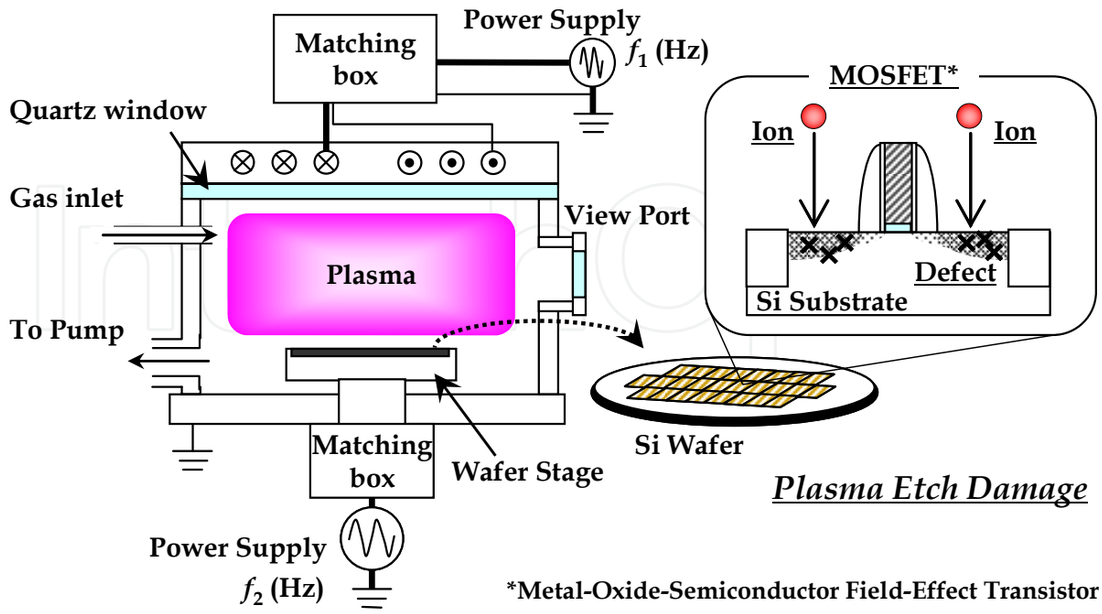

Fig. 2. Illustrations of plasma process reactor and plasma etch damage.

Since the number of particles to be simulated may be quite large (>10^{10} cm^{-3}) during plasma etching, classical MD simulations based on Newton's equation of motion (Graves & Humbird, 2002; Ohta & Hamaguchi, 2001a, 2001b) are now widely employed, compared to those using quantum mechanical calculations (Mazzarolo et al., 2001; Pelaz et al., 2009). Recently MD simulations have been used to understand formation of the surface "damaged" layer and displacement of Si atoms – PID (Graves & Humbird, 2002; Pelaz et al., 2009). However, the primary focus of these conventional MD simulations has been placed on the surface-reaction chemistry among ions, radicals, and the surface material. Since plasma etch processes are utilized for MOSFET fabrication, not only the surface reaction mechanism but also the effects of PID on MOSFET performance degradation should carefully be taken into account. Thus, MD simulations for PID should be incorporated with the prediction of electrical characteristics of MOSFETs.

There are two major challenging parts in the development of future MOSFET and plasma etch process: (1) A systematic and quantitative understanding of PID – the thickness of the damaged layer and the density of the displaced Si atoms (defects), and (2) A comprehensive design framework for future plasma by considering the effect of PID on electrical characteristics of MOSFETs. By keeping these issues in mind, this chapter discusses PID mechanisms by a classical MD simulation. We compare the simulation results with experimental data obtained by various analysis techniques. Future key issues concerning the effects of PID on MOSFET performance are provided. This chapter is organized as follows: In Sec. 2, we review the PID mechanism (Si loss mechanism – Si recess structure formation as mentioned later). In Sec. 3, the MD simulation employed in this study is briefly described. In Sec. 4, the simulation results are presented. In Sec. 5, experimental results are compared to the simulation results. Concluding remarks are in Sec. 5.

2. Ion-bombardment damage to MOSFET during plasma processing

Figure 3 illustrates a PID mechanism induced by the ion bombardment on Si surface during an offset spacer (SIA, 2009) etching (one of manufacturing steps) for MOSFET. During plasma etching, an energetic ion impinges on the Si surface with an energy of E_{ion}, leasing the energy by a series of collisions, then, it creates the defect sites under the exposed surface. This mechanism forms the damaged layer. In general, defect sites in Si substrate are referred to as displaced Si atoms, vacancies, and interstitials. As seen on the right in Fig. 3, the damaged structure consists of the surface (amorphous) and interfacial (a mixture of amorphous and crystalline structure) layers. Underneath these layers, there exist (latent) localized defect sites. (In this study, we denote these sites as "(local) defect sites".) The surface and interfacial layers can usually be monitored by an optical technique such as spectroscopic ellipsometry (SE) in production lines. The profile of defect site and the thickness of damaged-layer are determined by E_{ion} as well as the potential between Si and the incident ion.

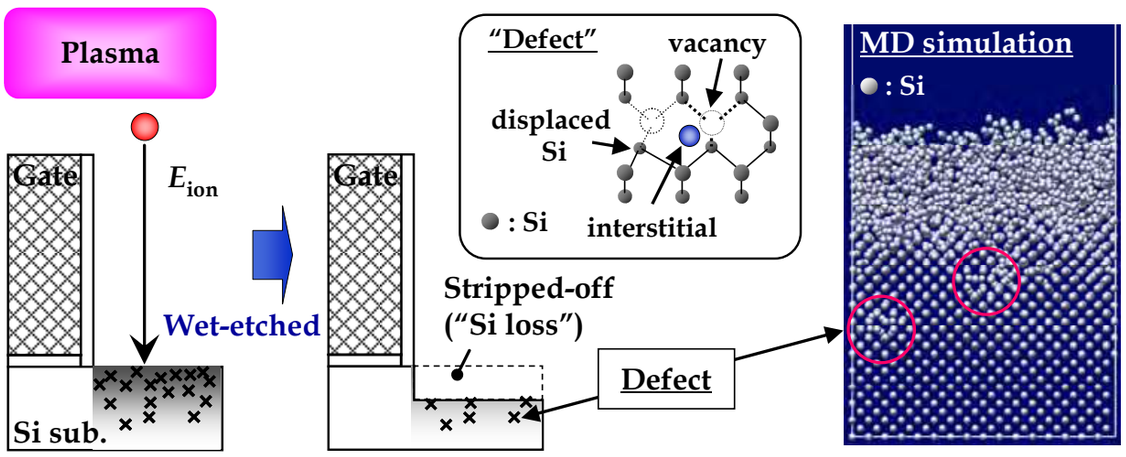

Fig. 3. Mechanism of plasma-etch damage to Si substrate and "Si loss" formation. Energetic ion bombardment creates a damaged layer underneath the Si surface. As shown on the right, localized defect sites are formed. A portion of the damaged layer with defect sites is stripped off during a subsequent wet-etch process, resulting in Si loss. (For details, see the text.)

In conventional MOSFET fabrication processes, a wet-etch step then follows the plasma etch process to remove the contaminated layer including the damaged layer. Since the damaged layer oxidizes due to an air exposure after the plasma etch, the portion is stripped off by the wet-etch. Then, the etched layer results in Si loss whose structure is observed as recessed Si surface, called "Si recess" (Ohchi et al., 2008; Petit-Etienne et al., 2010; Vitale & Smith, 2003). Si recess is formed in the source / drain extension (SDE) region in a MOSFET.

It has been reported (Eriguchi et al., 2009a; Eriguchi et al., 2008a) that the Si recess structure by PID degrades MOSFET performance, i.e., induces the shift of threshold voltage (V_{th}) for MOSFET operation. Since V_{th} (Sze, 1981; Sze & Ng, 2007) plays an important role in determining the performance, Si recess structure has become a primal problem in the present-day MOSFET development (SIA, 2009). To understand the formation of Si recess

structure (PID), the damage creation mechanism should be clarified from both theoretical and experimental viewpoints. Moreover, to predict the effects of PID on the MOSFET electrical characteristics, the defect structures should be identified quantitatively with high accuracy. In this study, we performed a classical molecular dynamics simulation as well as quantitative analyses of the local defect site density. Then, we discuss the effects of PID on the electrical characteristics of MOSFET.

3. Molecular dynamics simulation for plasma etching

Regarding to classical MD simulations for plasma etch process, many papers have been focusing on the surface reactions to understand details of silicon and silicon dioxide etch characteristics by energetic halogen (Abrams & Graves, 2000; Hanson et al., 1997; Humbird & Graves, 2004; Nagaoka et al., 2009; Ohta & Hamaguchi, 2001b) and fluorocarbon (Abrams & Graves, 1999) ions. The primal focuses are placed on estimation of etch yield by incident ions and the selectivity for RIE system. Regarding the ion bombardment damage, Graves and Humbird (Graves & Humbird, 2002) have reported in detail the formation of damaged layer in crystalline Si structures by Ar ion impacts. They estimated a stopping range of ions as well as a thickness of the amorphous (amorphized) layer formed near the surface. However, the detail mechanism of local defect site formation was not discussed.

As mentioned in Sec. 1, an RIE system includes the physical and chemical reactions triggered by 10 – 10^3 eV high-energy ion impacts. Although *ab initio* MD simulations are now available, they cannot be applied in practice. This is because more than 10^3 atoms are necessary to construct a solid surface and the total number of incident ions is more than 10^{10} cm^{-2}, resulting in more than 10^3 impacts on the surface with the area of 10 nm^2 (~ commonly simulated size). Therefore, at present, the only possible candidate for atomistic RIE simulations is a classical MD, in particular, with pre-constructed interatomic potential functions.

One of the commonly used interatomic potential functions for Si-containing systems is the one proposed by Stillinger and Weber (SW) (Stillinger & Weber, 1985) wherein the total potential energy consists of two- and three-body functions. The SW potential function was originally designed for Si/F systems. Afterwards various potential sets for Si/Cl (Ohta & Hamaguchi, 2001b), Si/O (Watanabe et al., 1999), Si/O/F (Ohta & Hamaguchi, 2001a), Si/O/Cl (Ohta & Hamaguchi, 2001a), and Si/O/C/F (Ohta & Hamaguchi, 2004; Smirnov et al., 2007) systems were provided. The other widely used function was proposed by Tersoff (Tersoff, 1988a, 1988b) with bond-order parameters including multi-body interactions. This potential can be effectively applied to C-containing systems to understand the complicated behaviours by the strengths of double and triple bonds. The parameter sets were proposed for systems including Si, C, Si/C, C/H, C/F, and Si/C/F (Abrams & Graves, 1998; Tanaka et al., 2000). In addition to the SW and Tersoff potential functions, other potential functions (Biswas & Hamann, 1987; Dodson, 1987; Hanson et al., 1997) were also proposed. Although there have been many discussions on the validity of the functions (Balamane et al., 1992), all of these functions can effectively reproduce some structural and thermodynamic characteristics of the materials and the relevant structural chemistry for some selected molecules. In this study, to eliminate complicated surface reactions usually occurring in halogen-containing plasmas, we focus on Ar-Si-O system for studying PID. We used the SW potential function for the Si-Si and Si-O systems.

3.1 Interatomic potential functions used in this study

The Stillinger-Weber potential function (Stillinger & Weber, 1985) utilizes both two-body and three-body interaction terms to stabilize the diamond cubic structure of crystalline silicon. The potential function is given by

$$\Phi = \sum_{i<j} V_2(i,j) + \sum_{i<j<k} V_3(i,j,k) \tag{1}$$

where $V_2(i, j)$ is the two-body interaction term between i-th and j-th atoms expressed as

$$V_2(i,j) = A_{ij} \cdot g_{ij}(B_{ij} \cdot r_{ij}^{-p_{ij}} - r_{ij}^{-q_{ij}}) \cdot \exp\left(\frac{C_{ij}}{r_{ij} - a_{ij}}\right), \tag{2}$$

if $r_{ij} < a_{ij}$, where a_{ij} is the cut-off distance, and $V_2(i, j) = 0$ otherwise. r_{ij} is the interatomic distance between i-th and j-th atoms in the SW's length unit (0.20951 nm). The parameters A_{ij}, B_{ij}, C_{ij}, p_{ij}, and a_{ij} depend only on the species of i-th and j-th atoms. g_{ij} (< 1) is the bond-softening function introduced by Watanabe et al. (Watanabe et al., 1999), adjusting the contribution of the two-body term to reproduce the cohesive energies of Si-O bonds. The three-body interaction term has the following form.

$$V_3(i,j,k) = h(r_{ij}, r_{ik}, \theta_{jik}) + h(r_{ji}, r_{jk}, \theta_{ijk}) + h(r_{ki}, r_{kj}, \theta_{ikj}), \tag{3}$$

where θ_{ijk} is the angle between two lengths of r_{ij} and r_{jk}, etc. Given that r_{ij} and r_{ik} are less than the cut-off distance, the function h is

$$h(r_{ij}, r_{ik}, \theta_{jik}) = \lambda_{jik} \exp\left(\frac{\gamma_{jik}^{ij}}{r_{ij} - a_{jik}^{ij}} + \frac{\gamma_{jik}^{ik}}{r_{ik} - a_{jik}^{ik}}\right) \times (\cos\theta_{jik} - \cos\theta_{jik}^0)^2, \tag{4}$$

otherwise $h = 0$. $\lambda_{jik}, \gamma_{jik}^{ij}, a_{jik}^{ij}, \gamma_{jik}^{ik}, a_{jik}^{ik}, \theta_{jik}$, and θ_{jik}^0 are parameters for the j-i-k triplet. a_{jik}^{ij} and a_{jik}^{ik} are the cut-off distances in the three-body configuration. For the "ideal" tetrahedral angle,

$$\cos\theta_{jik}^0 = -\frac{1}{3} \tag{5}$$

is held.

Regarding the two-body system with Ar, the Moliere-type repulsive pair potential function (Moliere, 1947; Torrens, 1972; Wilson et al., 1977) was employed. The potential function $V_2(i,j)$ includes a screening function $f_s(r_{ij})$ combined with a Coulomb potential. The function is expressed as

$$V_2(i,j) = \frac{Z_i Z_j e^2}{4\pi\varepsilon_0 r_{ij}} f_s(r_{ij}), \tag{6}$$

where e is the elementary charge, ε_0 is the permittivity of a vacuum, and Z_i and Z_j are the atomic numbers of the projectile (Ar) and target (Si, O, Ar) atoms, respectively. The expression of the screening function has been studied by many researchers (Torrens, 1972). So far, the repulsive interatomic potential between Ar and other elements has been modified (Wilson et al., 1977). In the expression of Moliere potential function, $f_s(r_{ij})$ is described as

$$f_s(r_{ij}) = \sum_{m=1}^{3} C_m \exp\left(-b_m r_{ij} / a'\right) = 0.35\exp\left(-\frac{0.3r_{ij}}{a'}\right) + 0.55\exp\left(-\frac{1.2r_{ij}}{a'}\right) + 0.10\exp\left(-\frac{6.0r_{ij}}{a'}\right) \quad (7)$$

where a' is the Firsov screening length (Firsov, 1957). The parameters proposed by Moliere (Moliere, 1947; Wilson et al., 1977) were used in this study.

3.2 Simulation procedure

We prepared a crystalline Si structure of squared Si (100) surface with a side length of 3.258 nm (six times of lattice constant ~ a squared 6-unit cell). The MD code used in this study was originally developed by Ohta and Hamaguchi (Ohta & Hamaguchi, 2001b). Each layer contained 72 atoms (= 1 monolayer (ML)). The bottom layer of the simulation cell (72 atoms) was rigidly fixed throughout the simulations. Initial depth of the simulation domain is 9-unit cells (nine times of lattice constant or 36 MLs). Periodic boundary condition was employed along the horizontal direction. Since a typical MOSFET structure has an SiO_2 layer on the Si substrate, the initial Si structure (6 × 6 × 9 cell) was "oxidized" before the Ar ion-bombardment. The oxidation was done by the 500-consecutive impacts of O atoms at 50 eV and followed by a subsequent cooling step with a set-point temperature of 400 K (See below). This step can create a surface oxidized layer corresponding to SiO_2 film formed on a source / extension region of MOSFET. Using the obtained SiO_2/Si structure, we injected Ar atoms with various incident energies. Ar atoms were injected from randomly selected horizontal locations above the surface of the cell at normal incidence. (In this study, we injected Ar ions with a constant E_{ion}, although, in practical plasma etching processes, the energy of ions obeys an ion energy distribution function (IEDF) dependent on a frequency of applied bias power (Lieberman & Lichtenberg, 2005) as illustrated in Fig. 2. However, a recent study (Eriguchi et al., 2010) showed that, in low applied bias voltages (< 500 eV), the average ion energy can be used as a primal measure for the damaged-layer thickness. Therefore, in the present MD simulation, we employed a mono-energetic ion impacts.) Note that, in plasma etching, an ion plays an important role in the reactions. However, in conventional MD simulations, charge-neutral atoms are used as incident particles. This is based on the assumption that incident ions are expected to be neutralized near the target surface due to a resonance or Auger process. Thus, in this study, we employed the above potential functions for charge-neutral Ar atom.

In the present-day RIE, plasma densities of the order of 10^9-10^{11} cm^{-3} are widely used. These densities lead to a (Bohm) flux of incident ions of 10^{13} – 10^{16} $cm^{-2}s^{-1}$, depending on the plasma density and the electron temperature (Lieberman & Lichtenberg, 2005). The interval between two successive ion impacts in the case of the present simulation domain (~ 10 nm^2) is much longer than the simulation time range. Therefore, each ion impact is thought to be an independent single event. To simulate such single events, for the first 0.7 ps after an energetic particle hits the surface, the motion of all particles in the domain are

solved numerically by a classical mechanics except for those in the rigidly fixed bottom layer. Then, we applied "artificial" cooling step to all the particles for 0.3 ps using Berendsen's heat removal scheme (Berendsen et al., 1984) with a cooling constant of 2.0 x 10^{-14} s^{-1}. The set-point temperature of the simulation cell was 400 K to reproduce the practical surface-temperature range during plasma etching. After the end of cooling step, a new energetic particle was directed again to the surface, and the whole simulation cycle was repeated. Details of the present MD simulation procedure were published elsewhere (Ohta & Hamaguchi, 2001b).

To evaluate the damage creation mechanisms, the defect structure formed by the ion impacts should be identified. Since comprehensive discussions on the defect structures may be beyond the scope of this article, we focus on the displaced Si atoms from the initial lattice site and the representative defect structures obtained by the simulations. To assign the displaced atoms, the Lindemann radius (r_L) was used as a measure of the displacement threshold (Hensel & Urbassek, 1998; Nordlund et al., 1998). The Lindemann radius is defined as the vibration amplitude of Si atoms at their melting point. For the SW potential function for Si, the radius is r_L = 0.45 Å. After the MD simulations, we inspected the displacements of all the Si atoms. Then, we identified all those atoms as defects if they were outside of the cubic cell (with an edge of $2 \times r_L$) whose center was located at an original lattice site. The number of the displaced atoms was counted to investigate an overall trend of PID in the course of successive ion impacts.

3.3 Simulation results and discussion

Figures 4 display typical damaged-layer/Si structures after 500 impacts by Ar ions with various energies. In these figures, Ar ions are omitted from the structures to clearly show the damaged layer and Si substrate. From other simulation results, we found that Ar atoms are usually present in the tetrahedral interstitial site underneath the interfacial layer. As seen in Fig. 4, the damaged layer thickness increases with an increase in E_{ion}. The heavily damaged surface layer and mixing layer with a rough interface (interfacial layer) are observed, in particular, for higher E_{ion} cases (≥ 200 eV). The surface layer has been usually identified as "an amorphous layer" in the view of simulation as discussed in previous literatures (Graves & Humbird, 2002; Oehrlein, 1989). However, when samples (wafers) are processed to the next manufacturing step, oxidation of the surface occurs due to an air exposure. As mentioned in the next section, the partially oxidized layer is detected by an optical technique as SiO_2 layer, and the residual damaged layer is evaluated as a mixing layer. In the following discussion, based on the experimental data, we define the surface amorphous layer and the rough interfacial region (including local defect sites) as the surface and interfacial layers, respectively. One should also pay careful attention to the local defect sites underneath the rough interface as highlighted in Fig. 4.

Regarding the local defect sites observed in Fig. 4, many respective structures have been proposed so far (Baraff et al., 1980; Batra et al., 1987; Cheng & Corbett, 1974; Estreicher et al., 1997; Hastings et al., 1997; Leung et al., 1999; Schober, 1989; Tang et al., 1997). In addition to vacancy, various interstitials have been studied extensively by *ab initio* calculations using clustered Si atoms. Tetrahedral and hexagonal interstitials as well as "dumbbell" and the bond-centered interstitial are commonly proposed structures (Batra et al., 1987; Leung et al., 1999). Figure 5 shows the profile of an increase in the number of Si atoms located in each

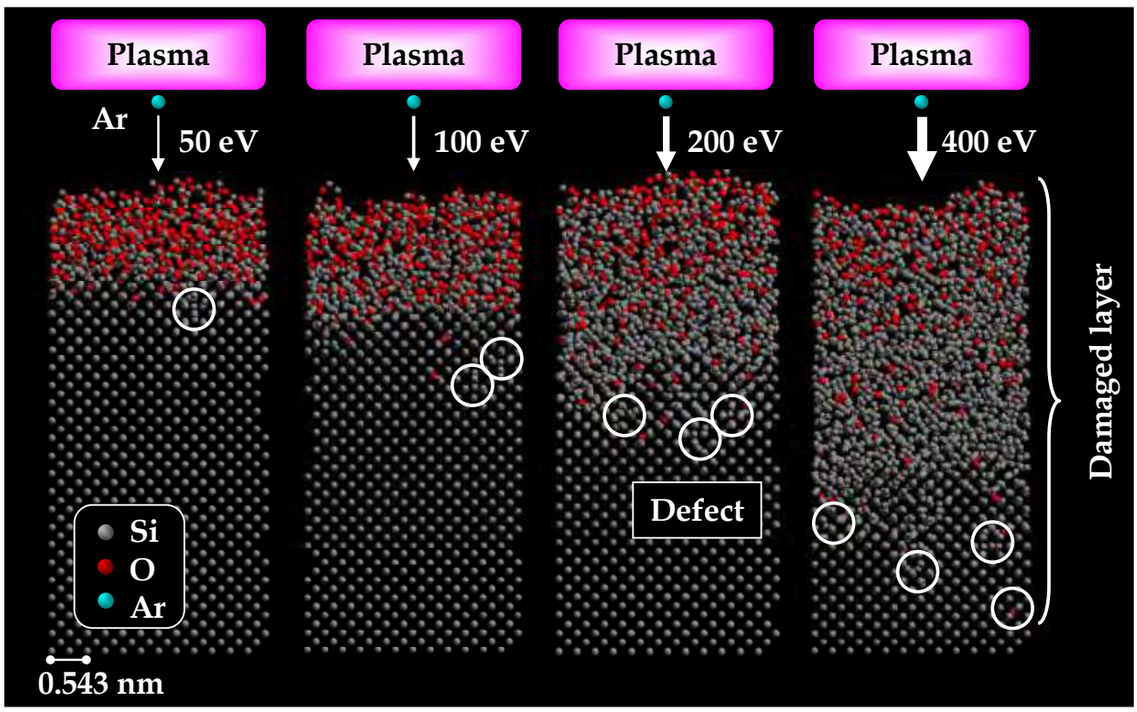

Fig. 4. SiO_2/Si structures after 500 impacts of Ar with different incident energies. The injected Ar ions are omitted from the cells for easy comparison. Local defect sites are highlighted.

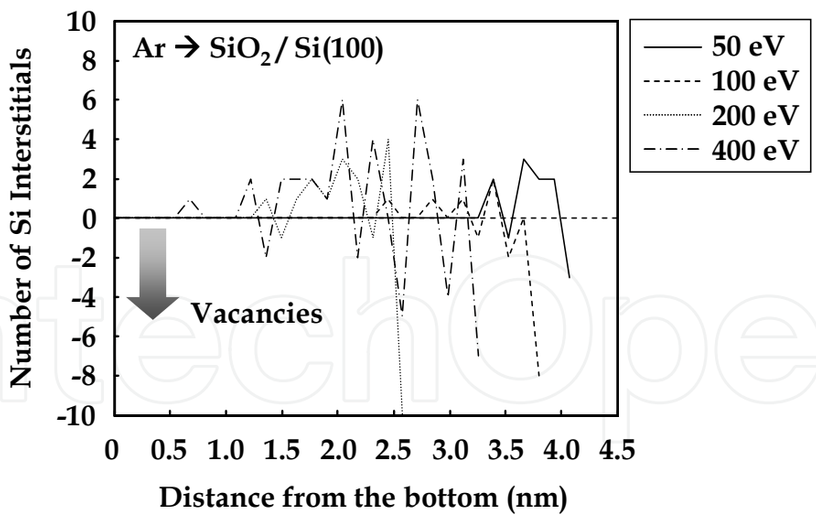

Fig. 5. Profiles of an increase in Si atoms in each atomic plane along [100].

atomic plane along the depth of [100] direction (The space between the planes is 0.13575 nm). 72-Si atoms are originally located in each plane for the present cell structure (6 × 6). In this figure, only Si atoms were inspected and counted. The difference in the interstitial structures mentioned in the above was not considered. The positive value presumably implies the presence of interstitials and the negative, that of vacancy. This means that the

local defect sites are consisting of vacancies as well as Si interstitials. (Note that one can see cumulatively the net positive value when integrating the data from the bottom. This implies that the Si interstitials are more probable than vacancies in those cases.) The interstitial Si atoms were formed by knock-on process.

By keeping in mind the results in Fig. 5, we investigated in detail some of typical defects in Fig. 4 to clarify the structures of these defects formed by PID. Figures 6 present some of typical structures – we chose three representative structures. On the left are shown the views of the defects on the (100) plane (along [100]). In the middle, the bird's views to the respective defects (Si atoms) are shown. Interstitial Si atoms are highlighted in the views. From Fig. 4, we roughly categorize the defect structures (the interstitial atoms) as Type-A, Type-B, and Type-C. Type-A is like a tetrahedral interstitial, and Type-B, a hexagonal interstitial (Batra et al., 1987; Leung et al., 1999; Schober, 1989). In both cases, neighbouring

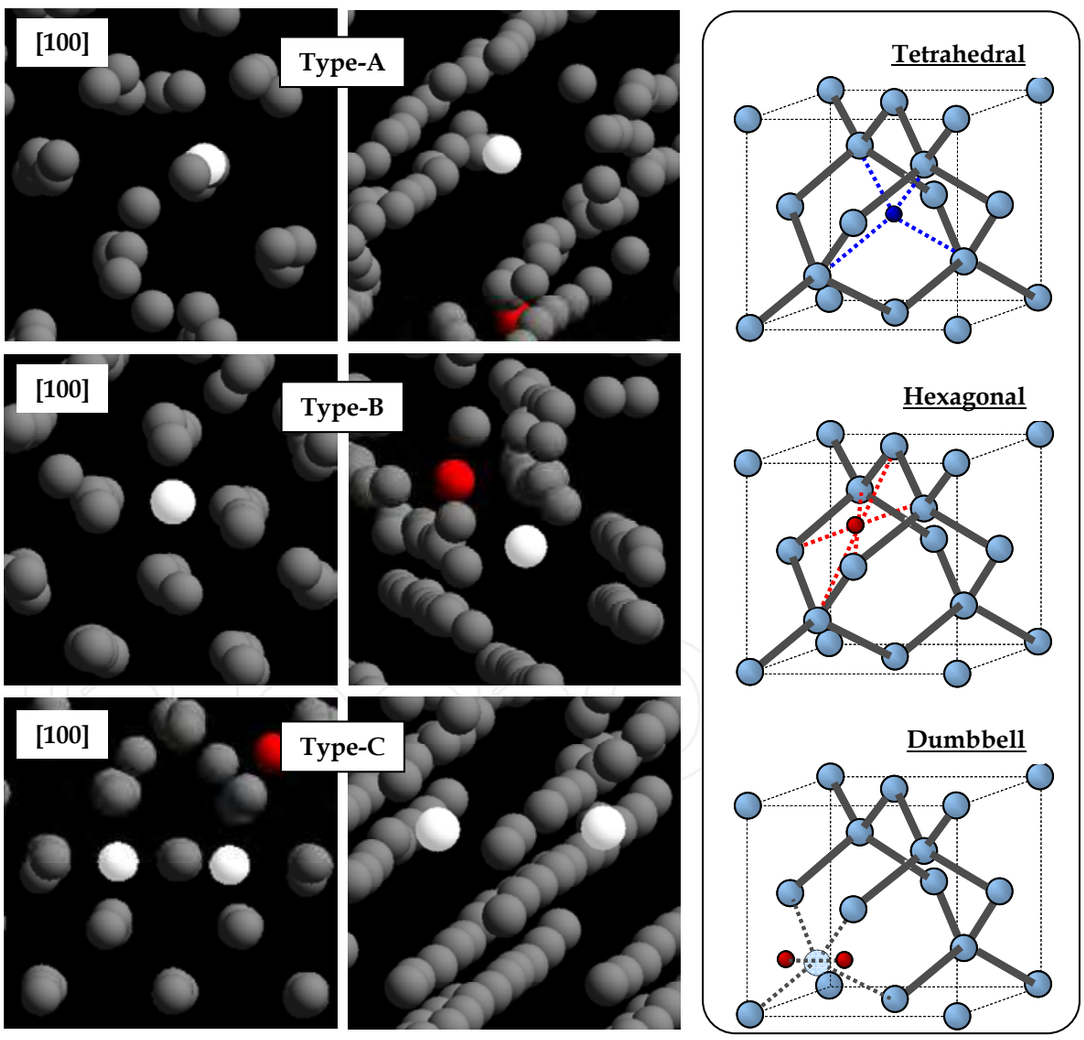

Fig. 6. Typical structures of Si-interstitial defects created by energetic ion bombardments. On the left are the views along [100] and the bird's-view are shown in the middle. On the right, typical structures assigned by previous reports are shown. (See also Fig. 4.)

Si atoms are not displaced considerably. Type-C is like a "dumbbell" structure where bonded Si atom was displaced from the lattice sites due to the presence of an interstitial Si permeating from other regions. It is widely believed that these structures are probable and found to be stable in terms of the formation energies calculated from a quantum mechanics scheme (Colombo, 2002; Leung et al., 1999; Tang et al., 1997). Typical structures reported so far are also illustrated on the right of Fig. 5. For details including other structures, please see the literatures (Batra et al., 1987; Cheng & Corbett, 1974; Leung et al., 1999). In terms of the effect of the presence of these structures on electrical characteristics of crystalline Si structure, it is also believed that these defects can create additional energy levels in the band gap ("band-gap states") (Estreicher et al., 1997; Hastings et al., 1997; Schultz, 2006). Therefore, one can speculate that the local defects by PID degrade MOSFET performance because the band-gap state plays a role as a carrier trap site inducing an increase in leakage current due to hopping conduction (Koyama et al., 1997) and/or an increase in a channel series-resistance (Eriguchi et al., 2009b) due to coulomb scattering by the trapped carrier. In general, it is difficult to identify those local defects by conventional analysis techniques such as TEM observation, in particular, to quantify the density of these defects. In the next section, by using novel analysis techniques, we quantify the density of the defects and discuss the electrical characteristics of these defects.

Since the observed defect structures are indeed derived from our MD simulations, we have to pay careful attention to the effects of the simulation procedure on our findings. In the present case, the number of defect sites (~ the density) might be dependent on both the simulation cell size and the number of Ar impacts. Conventional MD simulations for plasma etch processes employ; (1) periodic boundary condition and (2) the rigid fixed Si atoms at the bottom plane of the cell. Both technical restrictions may make the defect generation mechanism being dependent on the cell-size. It was reported (Abrams & Graves, 2000; Graves & Humbird, 2002) that the formation of amorphous layer is time-dependent, i.e., the number of ion impacts determines whether the damaged-layer formation process is in a growth or a saturation phases. Previous reports showed that the thickness of amorphous layer by Ar ion impacts became in a steady state after 1.5-monolayer (ML) impact (Graves & Humbird, 2002) and also that the reaction layer thickness by F ion impacts, after 10 MLs (Abrams & Graves, 2000).

Figure 7 shows at first the cell-size dependence of Si ion penetration depth. Si was self-implanted repeatedly with the energy of 150 eV into the initial simulation cells of various sizes. Due to a stopping process (Lindhard et al., 1963; Wilson et al., 1977), the injected Si atom loses the energy by a series of collisions and finally comes to rest in Si substrate. After 1000 impacts of Si atoms, the profiles of penetration depth ("projection range") were determined and compared for various cell sizes. As shown, one can see a small difference among the peak positions, i.e., the ion penetration depth is almost independent on the cell size. The result may suggest that one can use a smaller cell-size for plasma-etch MD simulation to reduce a "simulation cost" for estimating the ion penetration depth. However, as mentioned later, for investigating the density of local defect site, a smaller cell-size statistically contains a smaller number of local defect sites under the same number of ion impacts. Hence, although the estimation of ion penetration depth can be done by using a smaller cell size, a larger number of impacts should be conducted to investigate an overall feature of local defect site structures. In Sec. 4, we compare the number of defect sites in Fig. 4 with that obtained by the experiments.

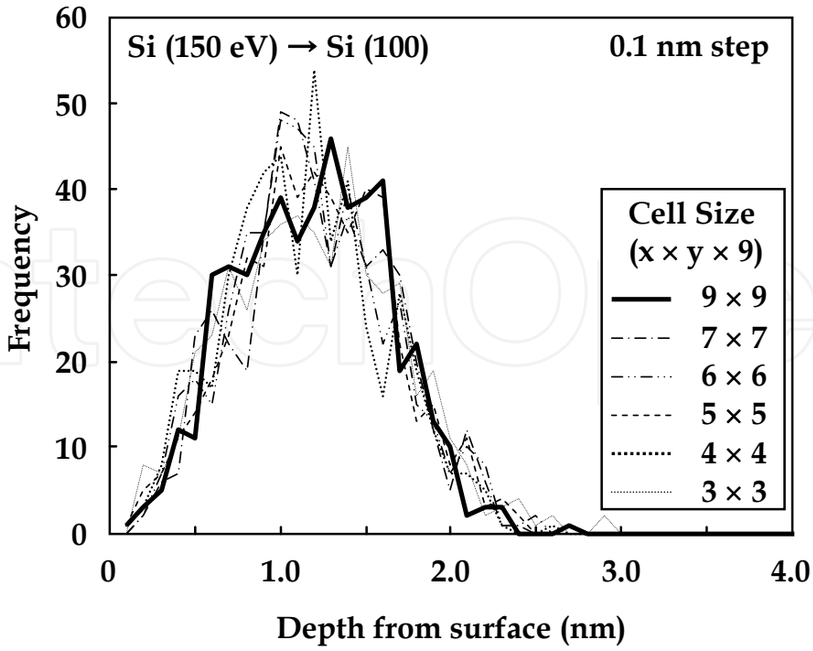

Fig. 7. Depth profiles of incident Si atoms into the cells with various sizes.

Figure 8 shows time evolutions of the number of displaced Si atoms (n_{Si}) determined from the algorithm based on the Lindemann radius, for the case of the present cell size of 6 × 6 × 9. As seen, at the initial stage, the counted n_{Si} increases with fluence until ~ 100 impacts, and then saturates after approximately 500 impacts for both E_{ion} cases. The 500-impact corresponds to ~ 7-ML injections in the case of the present (100) surface (6 × 6). Compared to previous reports (Abrams & Graves, 2000; Graves & Humbird, 2002), this saturation value is

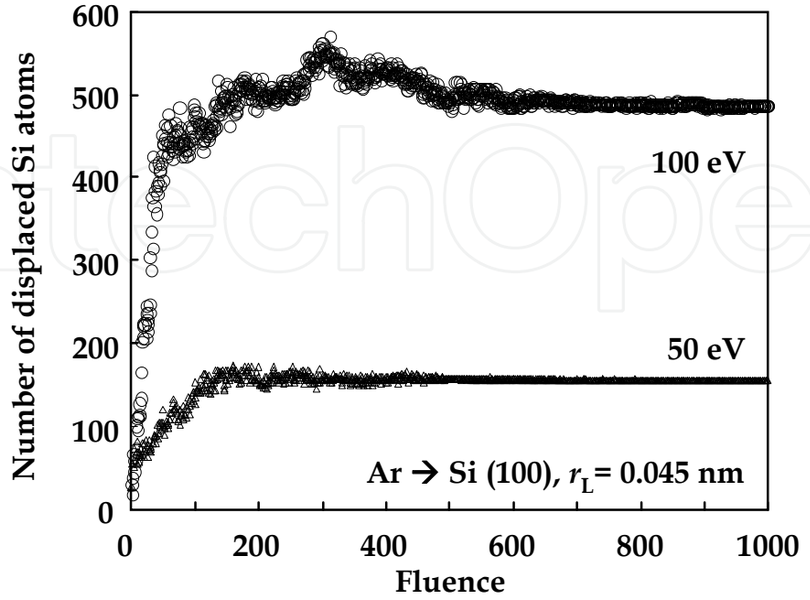

Fig. 8. Time evolutions of the number of displaced Si atoms.

in the reasonable range. Thus, it can be concluded that by considering the saturation phenomena, the number of impacts should be properly optimized in advance when performing plasma-etch MD simulations. (In Fig. 4, we have shown the results by 500 impacts for discussions on the defect sites.)

4. Comparison with experimental data

4.1 Experimental setup, test sample structure, and evaluation techniques

To verify the above MD simulation results, we carried out plasma treatments of Si wafers by using two plasma reactors. N-type (100) Si wafer with 0.02 Ωcm was exposed to an inductively coupled plasma (ICP) reactor (See Fig. 2) and a DC plasma reactor. In the ICP reactor (Eriguchi et al., 2008a), the plasma was generated by a source power supply unit. The applied power was 300 W. The plasma density can be controlled by changing this source power. On the other, a bias power applied to the wafer stage determines the energy of ion incident on the wafer surface. In the present study, the bias power was varied from 50 to 400 W. The frequencies of source and bias power were 13.56 MHz for both. Ar was used and the pressure was 20 mTorr. Unless otherwise specified, the process time was 30 s. By using an oscilloscope, we determined self dc bias (V_{dc}<0) and plasma potential (V_p), resulting in an average ion energy E_{ion} (eV) (= $e(V_p - V_{dc})$) ranging from 56 to 411 eV. From a Langmuir probe measurement, the electron density and the electron temperature were estimated to be 3.3×10^{11} cm^{-3} and 2.6 eV, respectively. Since Ar plasma is electropositive, the ion density is approximately equal to the electron density 3.3×10^{11} cm^{-3}, giving the flux of ions (Γ_{ion}) of 1.2×10^{17} $cm^{-2}s^{-1}$. Note that this ICP configuration results in a constant Γ_{ion} to the wafer for all bias power conditions in the present experiments.

In order to evaluate the damaged structure, we conducted several analyses – spectroscopic ellipsometry (SE) (Herman, 1996), high-resolution transmission electron microscope (HR-TEM) observation, Rutherford backscattering spectroscopy (HR-RBS), photoreflectance spectroscopy (PRS) (Herman, 1996), and capacitance – voltage (C-V) measurement. In particular, to quantify the local defect site density, we employed PRS and CV measurement.

In SE analysis, the damaged layer is assumed to consist of two regions, i.e., the surface and interfacial layers (abbreviated as SL and IL, respectively). The SL is composed of SiO_2, as a result of oxidation of heavily damaged regions by exposure to an air as well as the presence of knock-on oxygen from the surface oxide layer. (This is confirmed from the MD simulation results.) The IL is partially oxidized or disordered Si, which is identified by SE as a mixed layer consisting of crystalline Si and SiO_2 phases. Thus, an optical model assuming four layers (ambient, surface SiO_2 layer, interfacial layer, and Si substrate) was employed (Eriguchi et al., 2008a; Matsuda et al., 2010). In this analysis, the thicknesses of the surface (SL: d_{SL}) and interfacial [IL (SiO_2 + crystalline-Si): d_{IL}] layers and the composition (f_{Si}: component of crystalline-Si) were determined.

PRS is one of modulation spectroscopic techniques (Aspnes, 1973; Pollak & Shen, 1990), where the surface of the sample is modulated by a laser beam. The reflectance change by using a probe beam was monitored. In the present PRS, the amplitude of reflectance change ($\Delta R/R$) for the damaged sample was measured. A decrease in $\Delta R/R$ means the defect generation in the surface region of Si substrate (< 10 nm) (Murtagh et al., 1997;

Wada et al., 2000). Details for the basics of PRS analysis and experimental procedures were described elsewhere (Eriguchi & Ono, 2008). From the laser-power dependence of spectra, the areal defect site density (N_{dam} (cm^{-2})) can be estimated (Eriguchi & Ono, 2008; Nakakubo et al., 2010a).

For Capacitance – Voltage (C-V) analysis (Sze, 1981), we used a mercury probe system. The bias frequency was 1 MHz. To estimate the local defect site density, we investigated $1/C^2$-V curves of the damage samples (Eriguchi et al., 2008a). Details are mentioned later.

4.2 Experimental results and discussion

4.2.1 Thickness of the damaged-layer

Figure 9 shows the surface and interfacial thicknesses (d_{SL} and d_{IL}) identified by SE with an optimized four-layer model. The samples were treated by the ICP system by changing an applied bias power. The SE analysis assigns an increase in d_{IL} with the average ion energy E_{ion}, while d_{SL} does not exhibit a clear increase. This may be due to surface sputtering mechanism. Rutherford backscattering spectrometry (not shown here) identifies the presence of stoichiometric SiO_2 region in the SL, and the IL consisting of SiO_2 and *c*-Si phases (Eriguchi et al., 2008a). Figure 10 shows TEM observation results for various bias powers. Although it is difficult for the case of higher E_{ion} to assign the details of the damaged structures, one can observe the presence of interfacial layer below the surface layer. The estimated thickness was found to be consistent with the SE data (Eriguchi et al., 2008a; Matsuda et al., 2010). The roughness in the interfacial layer is confirmed to increase, in particular, for the 400-W case. The increase in roughness may agree with MD simulation results in Fig. 4. Therefore, it is concluded that the presence of both the surface and interfacial layers should be taken into account when evaluating the damaged-layer thickness by SE and/or TEM. Note that, from these TEM observation results, one can see no local defect site which was assigned by MD simulations. To identify these local defect sites, other novel techniques are required. In the subsection 4.2.3, we provide the results by these techniques.

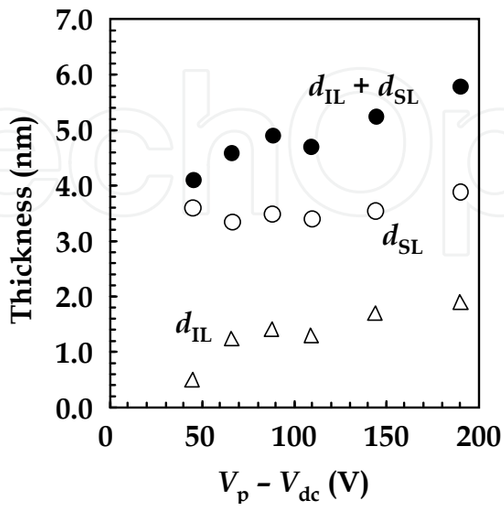

Fig. 9. Thicknesses of surface and interfacial layers obtained by spectroscopic ellipsometry with a four-layer optical model. Total optical thickness is also shown (closed circles).

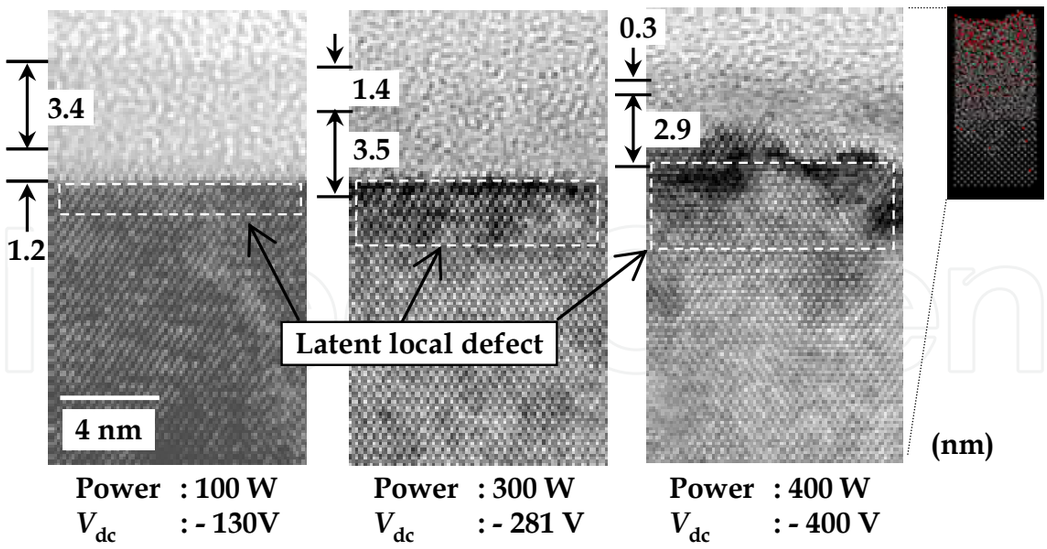

Fig. 10. TEM observation results for the Si wafer surface damaged by various bias powers.

4.2.2 Time-dependent damaged layer formation

As indicated in Fig. 8, the MD simulation predicts growth of the damaged layer in accordance with ion fluence. Some of experimental results regarding this phenomenon are shown in Fig. 11. Figure 11 indicates d_{SL} and d_{IL} as a function of process time (plasma exposure time t_{pro}). A DC plasma reactor was used to create PID for various conditions; V_{dc} = - 300 and - 350 V, respectively. Dependences of d_{SL} and d_{IL} on t_{pro} are shown. As t_{pro} increases, while the d_{SL} is almost constant (due to oxidation of surface layer by an air exposure), the d_{IL} increases for both cases. Moreover, the d_{IL} tends to saturate after a certain amount of time; 5 s for - 300 V and 10 s for - 350 V. From a Langmuir probe measurement, the electron temperature and the electron density were estimated to be 3.0 eV and ~ 10^9 cm^{-3}, respectively, giving Γ_{ion} of ~ 2 × 10^{14} $cm^{-2}s^{-1}$ in these experiments. Thus, the total dosage (fluence) is approximately 2 × 10^{15} cm^{-2} for 10 s. Based on the results by the MD simulations in Fig. 8, 500-impact in the present cell size corresponds to a fluence of ~ 5 × 10^{15} cm^{-2}. Although the E_{ion} in the DC plasma processes was not measured precisely (only deduced from applied DC bias voltages), we can speculate that the saturating behaviour of d_{IL} in Fig. 11 corresponds to the results in Fig. 8. In other words, once Γ_{ion} is properly determined by plasma diagnostics, the MD simulation can predict the time evolution of damaged-layer formation in practical plasma etching process.

In general, the number of ion impacts combined with the cell size is a more practical and useful measure rather than MLs for MD simulations, because the density of local defect site is a key parameter determining the effects of PID on MOSFET performance degradation. Figure 12 provides the relationship among the number of ion impacts, Γ_{ion}, and t_{pro}. Figure 12 guides how many ion impacts are necessary in MD simulations to predict correctly the local defect site generation during practical plasma etching. For a given Γ_{ion}, the number of impacts in a MD simulation should be increased with an increase in t_{pro}. For example, in the case of Γ_{ion} = 10^{15} $cm^{-2}s^{-1}$ and t_{pro} = 10^2 s, approximately a 10000–impact is needed in the MD simulation. Note that this value is dependent on the cell size. Deduced only from the time

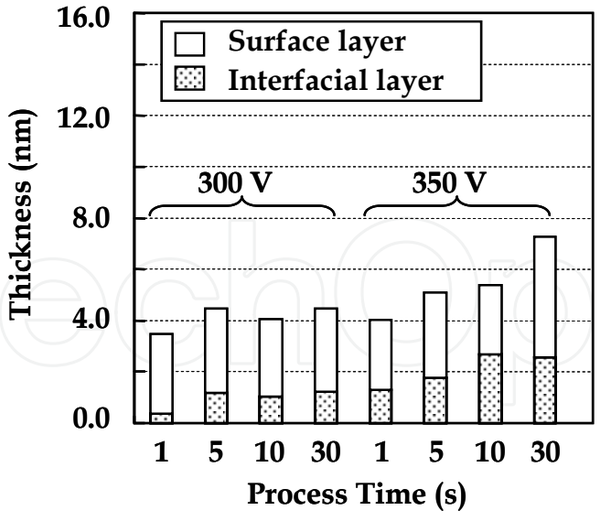

Fig. 11. Thicknesses of surface and interfacial layers as a function of process time. A DC plasma reactor was used.

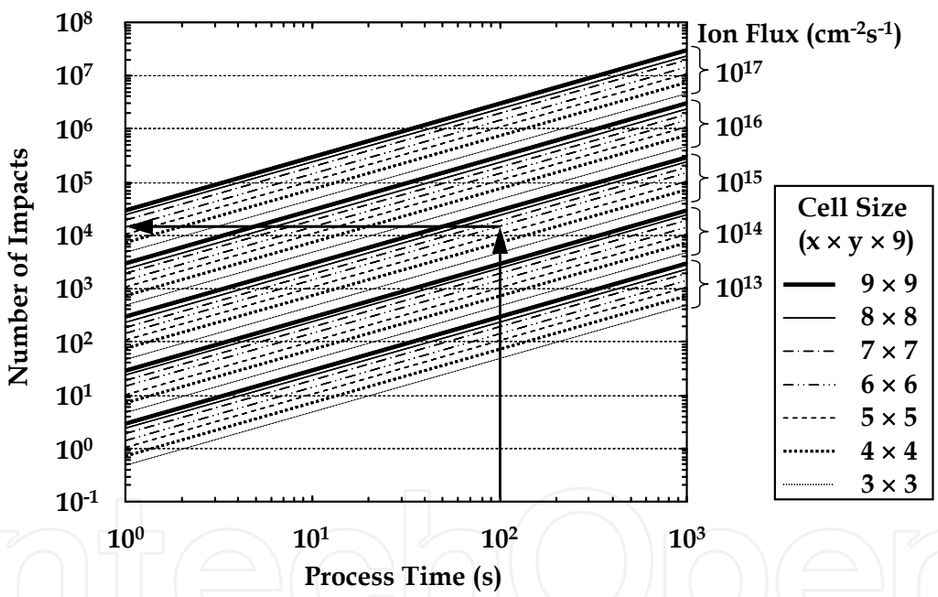

Fig. 12. The number of impacts required for MD simulation to predict practical plasma etch damage for various ion fluxes. The cell size dependence is shown by the respective lines.

evolution of damaged-layer formation as in Fig. 8, one can expect that a smaller size is better (more efficient). However, as discussed in the next, in terms of local defect site density, one has to increase a cell size as much to understand accurate pictures and overall features of the defect structures for the precise prediction of MOSFET performance degradation.

4.2.3 Density of defect sites

So far, PID has been evaluated by a wide variety of techniques (Awadelkarim et al., 1994; Egashira et al., 1998; Kokura et al., 2005; Mu et al., 1986; Oehrlein et al., 1988; Yabumoto et

al., 1981). However, there have been not so many reports quantifying the density of created local defects by PID. In this study, we employed two different quantification techniques, photoreflectance spectroscopy (PRS) and capacitance-voltage (C-V) measurement. Details are presented in other literatures (Eriguchi et al., 2008a; Eriguchi & Ono, 2008).

Figure 13 shows the estimated local defect site density from photoreflectance spectra of the test structures damaged by the ICP system (closed squares, on the left axis). By using a modified PRS model for estimation of the density of defect sites (Eriguchi et al., 2008b; Eriguchi & Ono, 2008), one can determines the areal defect site density (N_{dam}) as a function of E_{ion}. From this figure, one can observe N_{dam} of the order of 10^{12} cm^{-2} for the present plasma conditions.

Figure 14 shows examples of $1/C^2$-V analysis results. Figure 14 on the right illustrates the basics of this C-V technique, where w and q are the depletion layer width and the elementary charge, respectively. By using a mercury probe system, a bias voltage applied to Si substrate was swept, and the capacitance was measured. We performed this C-V measurement for both the control (without plasma exposure) and the damaged samples. When the value $1/C^2$ is plotted along the bias voltage (V_b) for a fresh Si substrate (the control), the slope of $1/C^2$ - V_b becomes constant since the slope corresponds to the impurity (dopant) concentration n_D (Goodman, 1963; Sze & Ng, 2007). For the plasma-damaged sample, one can see the distortion of $1/C^2$ - V_b curves in the inversion region as seen on the left figure. In this experiment, we used n-type Si substrate, thus, the negative bias voltage ($V_b < 0$)) corresponds to the inversion layer formation region. The presence of the local defect site (carrier trapping site) causes doping loss (a decrease in n_D) by intermixing with subsequently-implanted ions (Kokura et al., 2005). Therefore, the distortion (a decrease in the slope of $1/C^2$ - V_b plot) indicates a defect site creation in the Si substrate. On the right in Fig. 14, the schematic view of these defect sites in the inversion scheme is also shown. From a change of the slope, we can estimate the volume density of the defect site (n_{dam} cm^{-3}) by assuming that the effect impurity concentration equals to (n_D + n_{dam}) (Eriguchi et al., 2008a; Nakakubo et al., 2010b). The calculated n_{dam} is plotted on the right axis in Fig. 13 (open circles). The n_{dam} on the order of 10^{18}-10^{19} cm^{-3} is assigned. Since the thickness of d_{IL} containing n_{dam} is estimated to be a few nanometers as seen in Fig. 9, the areal density calculated from the E_{ion}-dependence of n_{dam} is consistent with N_{dam} by PRS. (Exactly speaking, the depth profile of n_{dam} should be taken into account, though.) One of the other important findings in Figs. 13 and 14 is the fact that the identified local defect sites are electrically active and may induce the MOSFET performance degradation. The defect site structures observed in Fig. 6 are fatal and should be investigated with carefully attention.

The estimated range of n_{dam} or N_{dam} gives an important interpretation to the MD simulations for PID as follows. The areal density of defect site ranging from 10^{12} to 10^{13} cm^{-2} in practical samples is equivalent to the number of defect site of 0.1 to 1 in the present 6 × 6 simulation cell (~ 10 nm^2), although it depends on t_{pro} and plasma parameters. In Fig. 4, the observed local defect sites are indeed a few in the number. This number corresponds to approximately 10^{13} cm^{-2} in practical samples, which is in consistent with the experimental results in Fig. 13. If one uses a smaller simulation size such as 3 × 3 cell to reduce the simulation cost, one can not find any defect sites statistically. In other words, a simulation scheme using a smaller size (for reducing the calculation time) may bring an erroneous conclusion (no observation of local defect sites). Regarding PID by MD, an optimization of the cell size in accordance with the plasma etching parameter such as Γ_{ion} is quite important.

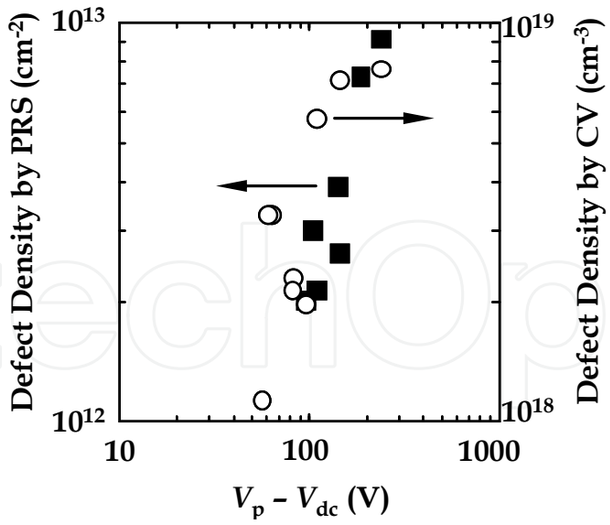

Fig. 13. Estimated defect site densities as a function of (V_p – V_{dc}) by two different analysis techniques; PRS and CV. From PRS, the areal density was determined, while, from CV, the volume density.

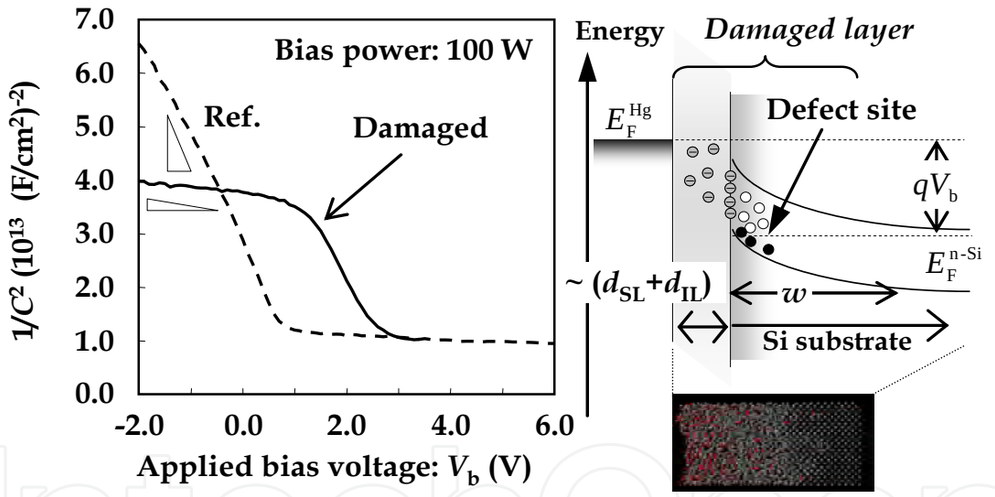

Fig. 14. Illustrations of an example for $1/C^2$-V plots and the energy band diagram during the CV measurement.

4.2.4 Prediction framework for MOSFET performance degradation by MD

Finally we discuss the effects of PID observed in the MD simulations and experimental data on MOSFET performance degradation. From the findings in the above, we can summarize the following key issues:

1. The damaged layer is found to consist of two layers, the surface and the interfacial layers. By considering this oxidation process, this thickness of Si loss (Si recess depth d_R) can be predicted by MD simulations.
2. Underneath the interfacial layer, local defect sites are present. The local defect structures can be assigned from MD simulations.

3. The local defect sites (observed in the MD simulation) are confirmed to be electrically active from the experimental data.

As proposed by Eriguchi et al.(Eriguchi et al., 2009a; Eriguchi et al., 2009b), Si recess depth d_R and the local defect sites degrades MOSFET-operation parameters such as V_{th} and I_d, where I_d is drain current determining the operation speed (Sze, 1981). These mechanisms are analytically expressed as,

$$\Delta V_{th} \propto -\frac{A}{L_g} d_R \,, \tag{8}$$

$$I_d = I_d^0 \cdot (1 - B \cdot n_{dam}) \,, \tag{9}$$

where ΔV_{th} and I_d^0 are the shift of threshold voltage and the drain current of a fresh device, respectively. A and B are the process- and device-structure-dependent parameters which can be determined from Technology Computer-Aided-Design (TCAD) simulations (Eriguchi et al., 2008a). A prediction of MOSFET performance from process parameters such as E_{ion} was demonstrated by using experimental relationship between E_{ion} and d_R (or n_{dam}). Moreover, from the present studies, one presumes that d_R and n_{dam} can be determined from MD simulations. At present, the statistical distribution functions for the local defect structures by PID are not clarified yet. A future work is hoped to assign the defect generation mechanisms and the statistical distribution functions with a help of MD simulations. Since the size of MOSFET is shrinking aggressively, a prediction framework of future device design can be organized by an atomistic technique such as MD simulations.

5. Conclusion

We applied classical MD simulations to investigate plasma-etch damage mechanisms. The simulated structures were found to consist of two layers, the surface and the interfacial layers. Due to oxidation by an air exposure, these two layers were identified in practice as SiO_2 and a mixed layer consisting of crystalline Si and SiO_2 phases, respectively. Underneath the interfacial layer, we assigned local defect sites, and the structures were confirmed to include typical Si interstitials. From the experiments, these sites were found to be electrically active. Combined with plasma diagnostics and quantitative analysis techniques of the local defect site density, the number of required ion impacts and the cell size for MD simulations were optimized for PID. Finally, a prediction framework for MOSFET design was discussed. An optimized MD simulation will be a promising candidate for predicting MOSFET performance degradation by PID.

6. Acknowledgment

The author greatly thanks Dr. H. Ohta for his great support of the MD simulation in this work. Acknowledgements are also given to Mr. Y. Nakakubo, Mr. A. Matsuda, Dr. Y. Takao, and Prof. K. Ono at Kyoto University, and Drs. M. Yoshimaru, H. Hayashi, S. Hayashi, H. Kokura, T. Tatsumi, and S. Kuwabara at STARC (Semiconductor Technology Academic Research Center) for their helpful discussions. This work was financially supported in part by STARC and a Grant-in-Aid for Scientific Research (B) from the Japan Society for the Promotion of Science.

7. References

Abrams, C., & Graves, D. (1998). Energetic ion bombardment of SiO_2 surfaces: Molecular dynamics simulations, *J. Vac. Sci. Technol. A*, Vol.16, No.5, (1998), pp. 3006-3019

Abrams, C. F., & Graves, D. B. (1999). Molecular dynamics simulations of Si etching by energetic CF_3^+, *J. Appl. Phys.*, Vol.86, No.11, (1999), pp. 5938-5948

Abrams, C. F., & Graves, D. B. (2000). Molecular dynamics simulations of Si etching with energetic F^+: Sensitivity of results to the interatomic potential, *J. Appl. Phys.*, Vol.88, No.6, (2000), pp. 3734-3738

Aspnes, D. E. (1973). Third-derivative modulation spectroscopy with low-field electroreflectance, *Surf. Sci.*, Vol.37, (1973), pp. 418-442

Awadelkarim, O. O., Mikulan, P. I., Gu, T., Reinhardt, K. A., & Chan, Y. D. (1994). Electrical properties of contact etched p-Si: A comparison between magnetically enhanced and conventional reactive ion etching, *J. Appl. Phys.*, Vol.76, No.4, (1994), pp. 2270-2278

Balamane, H., Halicioglu, T., & Tiller, W. A. (1992). Comparative study of silicon empirical interatomic potentials, *Phys. Rev. B*, Vol.46, No.4, (1992), pp. 2250-2279

Baraff, G. A., Kane, E. O., & Schluter, M. (1980). Theory of the silicon vacancy: An Anderson negative-U system, *Phys. Rev. B*, Vol.21, No.12, (1980), pp. 5662-5986

Batra, I. P., Abraham, F. F., & Ciraci, S. (1987). Molecular-dynamics study of self-interstitials in silicon, *Phys. Rev. B*, Vol.35, No.18, (1987), pp. 9552-9558

Berendsen, H. J. C., Postma, J. P. M., Gunsteren, W. F. v., DiNola, A., & Haak, J. R. (1984). Molecular dynamics with coupling to an external bath, *J. Chem. Phys.*, Vol.81, No.8, (1984), pp. 3684-3690

Biswas, R., & Hamann, D. R. (1987). New classical models for silicon structural energies, *Phys. Rev. B*, Vol.36, No.12, (1987), pp. 6434-6445

Cheng, L.-J., & Corbett, J. W. (1974). Defect creation in electronic materials, *Proceedings of the IEEE*, Vol.62, No.9, (1974), pp. 1208-1214

Colombo, L. (2002). Tight-Binding Theory of Native Point Defects in Silicon, *Annual Review of Materials Research*, Vol.32, No.1, (2002), pp. 271-295

Dodson, B. W. (1987). Development of a many-body Tersoff-type potential for silicon, *Phys. Rev. B*, Vol.35, No.6, (1987), pp. 2795-2798

Egashira, K., Eriguchi, K., & Hashimoto, S. A new evaluation method of plasma process-induced Si substrate damage by the voltage shift under constant current injection at metal/Si interface, *IEDM Tech. Dig.*, pp. 563-566, San Francisco, CA, USA, Dec 06-09, 1998

Eriguchi, K., Matsuda, A., Nakakubo, Y., Kamei, M., Ohta, H., & Ono, K. (2009a). Effects of Plasma-Induced Si Recess Structure on n-MOSFET Performance Degradation, *IEEE Electron Device Lett.*, Vol.30, No.7, (2009), pp. 712-714

Eriguchi, K., Nakakubo, Y., Matsuda, A., Kamei, M., Ohta, H., Nakagawa, H., S. Hayashi, Noda, S., Ishikawa, K., Yoshimaru, M., & Ono, K. A New Framework for Performance Prediction of Advanced MOSFETs with Plasma-Induced Recess Structure and Latent Defect Site, *IEDM Tech. Dig.*, pp. 443-446, San Francisco, CA, USA, Dec 15-17, 2008

Eriguchi, K., Nakakubo, Y., Matsuda, A., Takao, Y., & Ono, K. (2009b). Plasma-Induced Defect-Site Generation in Si Substrate and Its Impact on Performance Degradation in Scaled MOSFETs, *IEEE Electron Device Lett.*, Vol.30, No.12, (2009), pp. 1275-1277

Eriguchi, K., Nakakubo, Y., Matsuda, A., Takao, Y., & Ono, K. (2010). Model for Bias Frequency Effects on Plasma-Damaged Layer Formation in Si Substrates, *Jpn. J. Appl. Phys.*, Vol.49, (2010), pp. 056203

Eriguchi, K., Ohno, A., Hamada, D., Kamei, M., & Ono, K. (2008b). Estimation of defect generation probability in thin Si surface damaged layer during plasma processing, *Thin Solid Films*, Vol.516, No.19, (2008), pp. 6604–6608

Eriguchi, K., & Ono, K. (2008). Quantitative and comparative characterizations of plasma process-induced damage in advanced metal-oxide-semiconductor devices, *J. Phys. D*, Vol.41, No.2, (2008), pp. 024002

Estreicher, S. K., Hastings, J. L., & Fedders, P. A. (1997). The ring-hexavacany in silicon: A stable and inactive defect, *Appl. Phys. Lett.*, Vol.70, No.4, (1997), pp. 432-434

Firsov, O. B. (1957). Scattering of Ions by Atoms, *Soviet Physics JETP*, Vol.34, No.7, (1957), pp. 308-311

Goodman, A. M. (1963). Metal - Semiconductor Barrier Height Measurement by the Differential Capacitance Method - One Carrier System, *J. Appl. Phys.*, Vol.34, No.2, (1963), pp. 329-338

Graves, D. B., & Humbird, D. (2002). Surface chemistry associated with plasma etching processes, *Appl. Surf. Sci.*, Vol.192, No.1-4, (2002), pp. 72-87

Hanson, D. E., Voter, A. F., & Kress, J. D. (1997). Molecular dynamics simulation of reactive ion etching of Si by energetic Cl ions, *J. Appl. Phys.*, Vol.82, No.7, (1997), pp. 3552-3559

Hastings, J. L., Estreicher, S. K., & Fedders, P. A. (1997). Vacancy aggregates in silicon, *Phys. Rev. B*, Vol.56, No.16, (1997), pp. 10215-10222

Hensel, H., & Urbassek, H. M. (1998). Implantation and damage under low-energy Si self-bombardment, *Phys. Rev. B*, Vol.57, No.8, (1998), pp. 4756-4763

Herman, I. P. (1996). *Optical Diagnostics for Thin Film Processing* (Academic Press), ISBN 0-12-342070-9, San Diego

Humbird, D., & Graves, D. B. (2004). Atomistic simulations of spontaneous etching of silicon by fluorine and chlorine, *J. Appl. Phys.*, Vol.96, No.5, (2004), pp. 791-798

Jin, W., Vitale, S. A., & Sawin, H. H. (2002). Plasma-surface kinetics and simulation of feature profile evolution in Cl_2 + HBr etching of polysilicon, *J. Vac. Sci. & Technol. A*, Vol.20, No.6, (2002), pp. 2106-2114

Kokura, H., Okabe, K., Nakaishi, M., & Miyajima, M. Plasma induced damage on ultra shallow junction in spacer etching, *Proc. Symp. Dry Process*, pp. 27-28, Jeju, Korea, Nov 28-30, 2005

Koyama, M., Cheong, C.-W., Yokoyama, K., & Ohdomari, I. (1997). Influence of Near-Surface Defects in Si Induced by Reactive Ion Etching on the Electrical Properties of the Pt/n-Si Interface, *Jpn. J. Appl. Phys.*, Vol.11, No.11, (1997), pp. 6682-6686

Leung, W. K., Needs, R. J., Rajagopal, G., Itoh, S., & Ihara, S. (1999). Calculations of Silicon Self-Interstitial Defects, *Phys. Rev. Lett.*, Vol.83, No.12, (1999), pp. 2351-2354

Lieberman, M. A., & Lichtenberg, A. J. (2005). *Principles of Plasma Discharges and Materials Processing*, (2nd ed., Wiley), ISBN 978-0-471-72001-0, New York

Lindhard, J., Scharff, M., & Schiott, H. E. (1963). Range Concepts and Heavy Ion Ranges, *Mat. Fys. Medd. K. Dan. Vidensk. Selsk.*, Vol.33, No.14, (1963), pp. 1-41

Matsuda, A., Nakakubo, Y., Takao, Y., Eriguchi, K., & Ono, K. (2010). Modeling of ion-bombardment damage on Si surfaces for in-line analysis, *Thin Solid Films*, Vol.518, No.13, (2010), pp. 3481-3486

Mazzarolo, M., Colombo, L., Lulli, G., & Albertazzi, E. (2001). Low-energy recoils in crystalline silicon: Quantum simulations, *Phys. Rev. B*, Vol.63, No.19, (2001), pp. 195207

Moliere, G. (1947). Theorie der Streuung schneller geladener Teichen I, *Z. Naturforschung*, Vol.A2, (1947), pp. 133-145

Mu, X. C., Fonash, S. J., Rohatgi, A., & Rieger, J. (1986). Comparison of the damage and contamination produced by CF_4 and CF_4/H_2 reactive ion etching: The role of hydrogen, *Appl. Phys. Lett.*, Vol.48, No.17, (1986), pp. 1147-1149

Murtagh, M., S M Lynch, Kelly, P. V., Hildebrandt, S., Herbert, P. A. F., Jeynes, C., & Crean, G. M. (1997). Photoreflectance characterization of Ar^+ ion etched and $SiCl_4$ reactive ion etched silicon (100), *Mat. Sci. Technol.*, Vol.13 (1997), pp. 961-964

Nagaoka, T., Eriguchi, K., Ono, K., & Ohta, H. (2009). Classical interatomic potential model for Si/H/Br systems and its application to atomistic Si etching simulation by HBr^+, *J. Appl. Phys.*, Vol.105, No.2, (2009), pp. 023302-023306

Nakakubo, Y., Matsuda, A., Kamei, M., Ohta, H., Eriguchi, K., & Ono, K. (2010a). Analysis of Si Substrate Damage Induced by Inductively Coupled Plasma Reactor with Various Superposed Bias Frequencies. In A. Amara & M. Belleville & T. Ea (Eds.), *Emerging Technologies and Circuits* (Vol. 66, pp. 107-120), London, (Springer)

Nakakubo, Y., Matsuda, A., Takao, Y., Eriguchi, K., & Ono, K. Study of Wet-Etch Rate of Plasma-Damaged Surface and Interface Layers and Residual Defect Sites, *Proc. Symp. Dry Process*, pp. 173-174, Tokyo, Japan, Nov 11-12, 2010

Nordlund, K., Ghaly, M., Averback, R. S., Caturla, M., Diaz de la Rubia, T., & Tarus, J. (1998). Defect production in collision cascades in elemental semiconductors and fcc metals, *Phys. Rev. B*, Vol.57, No.13, (1998), pp. 7556-7570

Oehrlein, G. S. (1989). Dry etching damage of silicon: A review, *Materials Sci. Eng. B*, Vol.4, No.1-4, (1989), pp. 441-450

Oehrlein, G. S., Bright, A. A., & Robey, S. W. (1988). X-Ray Photoemission Spectroscopy Characterization of Si Surfaces after CF_4/H_2 Magnetron Ion Etching - Comparisons to Reactive Ion Etching, *J. Vac. Sci. Technol. A*, Vol.6, No.3, (1988), pp. 1989-1993

Ohchi, T., Kobayashi, S., Fukasawa, M., Kugimiya, K., Kinoshita, T., Takizawa, T., Hamaguchi, S., Kamide, Y., & Tatsumi, T. (2008). Reducing Damage to Si Substrates during Gate Etching Processes, *Jpn. J. Appl. Phys.*, Vol.47, No.7, (2008), pp. 5324-5326

Ohta, H., & Hamaguchi, S. (2001a). Classical interatomic potentials for Si-O-F and Si-O-Cl systems, *J. Chem. Phys.*, Vol.115, No.14, (2001), pp. 6679-6690

Ohta, H., & Hamaguchi, S. (2001b). Molecular dynamics simulation of silicon and silicon dioxide etching by energetic halogen beams, *J. Vac. Sci. & Technol. A*, Vol.19, No.5, (2001), pp. 2373-2381

Ohta, H., & Hamaguchi, S. (2004). Effects of Van der Waals Interactions on SiO_2 Etching by CF_x Plasmas, *J. Plasma Fusion Res*, Vol.6, (2004), pp. 399-401

Pelaz, L., Marques, L. A., Aboy, M., Lopez, P., & Santos, I. (2009). Front-end process modeling in silicon, *The European Physical Journal B*, Vol.72, (2009), pp. 323-359

Petit-Etienne, C., Darnon, M., Vallier, L., Pargon, E., Cunge, G., Boulard, F., Joubert, O., Banna, S., & Lill, T. (2010). Reducing damage to Si substrates during gate etching processes by synchronous plasma pulsing, *J. Vac. Sci. & Technol. B*, Vol.28, No.5, (2010), pp. 926-934

Pollak, F. H., & Shen, H. (1990). Photoreflectance Characterization of Semiconductors and Semiconductor Heterostructures, *J. Electronic Materials*, Vol.19, No.5, (1990), pp. 399-406

Sankaran, A., & Kushner, M. J. (2004). Integrated feature scale modeling of plasma processing of porous and solid SiO_2. I. Fluorocarbon etching, *J. Vac. Sci. & Technol. A*, Vol.22, No.4, (2004), pp. 1242-1259

Schober, H. R. (1989). Extended interstitials in silicon and germanium, *Phys. Rev. B*, Vol.39, No.17, (1989), pp. 13013-13015

Schultz, P. A. (2006). Theory of defect levels and the "band gap problem" in silicon, *Phys. Rev. Lett.*, Vol.96, No.24, (2006), pp. 246401

SIA. (2009). *The International Technology Roadmap for Semiconductors 2009 edition, Front End Processes*

Smirnov, V. V., Stengach, A. V., Gaynullin, K. G., Pavlovsky, V. A., Rauf, S., & Ventzek, P. L. G. (2007). A molecular dynamics model for the interaction of energetic ions with SiOCH low-*k* dielectric, *J. Appl. Phys*, Vol.101, No.5, (2007), pp. 053307

Stillinger, F. H., & Weber, T. A. (1985). Computer simulation of local order in condensed phases of silicon, *Phys. Rev. B*, Vol.31, No.8, (1985), pp. 5262-5271

Sze, S. M. (1981). *Physics of Semiconductor Devices,* (2nd ed., Wiley), ISBN 0-471-05661-8, New York

Sze, S. M., & Ng, K. K. (2007). *Physics of Semiconductor Devices* (3rd ed., Wiley-Interscience), ISBN 978-0-471-14323-9, Hoboken, NJ

Tanaka, J., Abrams, C., & Graves, D. (2000). New C-F interatomic potential for molecular dynamics simulation of fluorocarbon film formation, *J. Vac. Sci. Technol. A*, Vol.18, No.3, (2000), pp. 938-945

Tang, M., Colombo, L., Zhu, J., & Diaz de la Rubia, T. (1997). Intrinsic point defects in crystalline silicon: Tight-binding molecular dynamics studies of self-diffusion, interstitial-vacancy recombination, and formation volumes, *Phys. Rev. B*, Vol.55, No.21, (1997), pp. 14279-14289

Tersoff, J. (1988a). Empirical interatomic potential for silicon with improved elastic properties, *Phys. Rev. B*, Vol.38, No.14, (1988), pp. 9902-9905

Tersoff, J. (1988b). New empirical approach for the structure and energy of covalent systems, *Phys. Rev. B*, Vol.37, No.12, (1988), pp. 6991-7000

Torrens, I. M. (1972). *Interatomic Potentials* (Academic Press, Inc.), New York

Tsuda, H., Miyata, H., Takao, Y., Eriguchi, K., & Ono, K. (2011). Three-Dimensional Atomic-Scale Cellular Model and Feature Profile Evolution during Si Etching in Chlorine-Based Plasmas: Analysis of Profile Anomalies and Surface Roughness, *Jpn. J. Appl. Phys.*, Vol.50, (2011), pp. 08JE06

Vitale, S. A., & Smith, B. A. (2003). Reduction of silicon recess caused by plasma oxidation during high-density plasma polysilicon gate etching, *J. Vac. Sci. Technol. B*, Vol.21, No.5, (2003), pp. 2205-2211

Wada, H., Agata, M., Eriguchi, K., Fujimoto, A., Kanashima, T., & Okuyama, M. (2000). Photoreflectance characterization of the plasma-induced damage in Si substrate, *J. Appl. Phys.*, Vol.88, No.5, (2000), pp. 2336-2341

Watanabe, T., Fujiwara, H., Noguchi, H., Hoshino, T., & Ohdomari, I. (1999). Novel Interatomic Potential Energy Function for Si, O Mixed Systems, *Jpn. J. Appl. Phys.*, Vol.38, No.4A, (1999), pp. L366-L369

Wilson, W. D., Haggmark, L. G., & Biersack, J. P. (1977). Calculations of nuclear stopping, ranges, and straggling in the low-energy region, *Phys. Rev. B*, Vol.15, No.5, (1977), pp. 2458-2468

Yabumoto, N., Oshima, M., Michikami, O., & Yoshii, S. (1981). Surface Damage on Si Substrates Caused by Reactive Sputter Etching, *Jpn. J. Appl. Phys.*, Vol.20, No.5, (1981), pp. 893-900

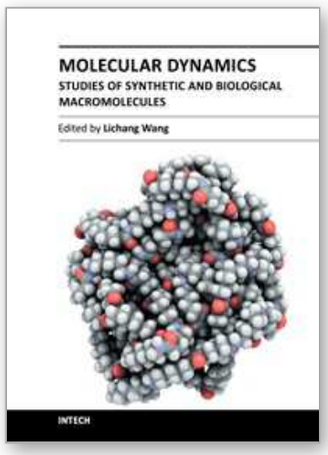

Molecular Dynamics - Studies of Synthetic and Biological Macromolecules

Edited by Prof. Lichang Wang

ISBN 978-953-51-0444-5
Hard cover, 432 pages
Publisher InTech
Published online 11, April, 2012
Published in print edition April, 2012

Molecular Dynamics is a two-volume compendium of the ever-growing applications of molecular dynamics simulations to solve a wider range of scientific and engineering challenges. The contents illustrate the rapid progress on molecular dynamics simulations in many fields of science and technology, such as nanotechnology, energy research, and biology, due to the advances of new dynamics theories and the extraordinary power of today's computers. This second book begins with an introduction of molecular dynamics simulations to macromolecules and then illustrates the computer experiments using molecular dynamics simulations in the studies of synthetic and biological macromolecules, plasmas, and nanomachines. Coverage of this book includes: Complex formation and dynamics of polymers Dynamics of lipid bilayers, peptides, DNA, RNA, and proteins Complex liquids and plasmas Dynamics of molecules on surfaces Nanofluidics and nanomachines

How to reference

In order to correctly reference this scholarly work, feel free to copy and paste the following:

Koji Eriguchi (2012). Application of Molecular Dynamics Simulations to Plasma Etch Damage in Advanced Metal-Oxide-Semiconductor Field-Effect Transistors, Molecular Dynamics - Studies of Synthetic and Biological Macromolecules, Prof. Lichang Wang (Ed.), ISBN: 978-953-51-0444-5, InTech, Available from: http://www.intechopen.com/books/molecular-dynamics-studies-of-synthetic-and-biological-macromolecules/application-of-molecular-dynamics-simulations-to-plasma-etch-damage-in-advanced-metal-oxide-semicond

InTech Europe
University Campus STeP Ri
Slavka Krautzeka 83/A
51000 Rijeka, Croatia
Phone: +385 (51) 770 447
Fax: +385 (51) 686 166
www.intechopen.com

InTech China
Unit 405, Office Block, Hotel Equatorial Shanghai
No.65, Yan An Road (West), Shanghai, 200040, China
中国上海市延安西路65号上海国际贵都大饭店办公楼405单元
Phone: +86-21-62489820
Fax: +86-21-62489821

IntechOpen